DOI: 10.1007/s12541-011-0109-5

Thermo-Mechanical Finite Element Analysis of Hot Judder Phenomenon of a Ventilated Disc Brake System

Sung Pil Jung[1], Tae Won Park[2,#], Jang Bom Chai[2] and Won Sun Chung[3]

1 Graduate School of Mechanical Engineering, Ajou University, Suwon, Gyeonggi-do, South Korea, 443-749
2 School of Mechanical Engineering, Ajou University, Suwon, Gyeonggi-do, South Korea, 443-749
3 Body Chassis Reliability Team, Korea Automotive Technology Institute, Chonan, Chungcheongnam-do, South Korea, 330-912
Corresponding Author / E-mail: park@ajou.ac.kr, TEL: +82-31-219-2952, FAX: +82-31-219-1965

KEYWORDS: Hot judder characteristics, Finite element model, Thermo-mechanical analysis, Brake dynamo test, Hot spot

Hot judder characteristics of a ventilated disc brake system are discussed. Three dimensional finite element models of the ventilated disc, pads and pistons are created, and a fully coupled thermo-mechanical analysis of the hot judder phenomenon of the disc brake system is performed using SAMCEF. The brake dynamo test is carried out according to the high speed judder test mode. The evolution of the temperature distribution on the disc surface is described, and the hot spot generation process is investigated. The simulation results such as the maximum disc temperature, BTV are compared to the data from the dynamo test, and the reliabilities of the analysis technique and simulation model presented in this paper are verified.

Manuscript received: December 14, 2010 / Accepted: March 31, 2011

1. Introduction

The friction heat generated between two sliding bodies causes thermoelastic deformation which alters the contact pressure distribution between the two bodies. This coupled thermo-mechanical process is referred to as frictionally-excited thermoelastic instability or TEI.[1] If the sliding speed is above the so called critical speed, the resulting thermo-mechanical feedback becomes unstable, leading to the developments of non-uniform contact pressure and local high temperature with important gradients called 'hot spots'.[2] The formation of such localized hot spots is accompanied by high local stresses that can lead to material degradation and eventual failure.[3] Also, the hot spots can be a source of undesirable frictional vibrations, known in the automotive disc brake community as 'hot roughness' or 'hot judder'.[4]

Numerous studies have been devoted to the analysis of thermoelastic instability. Barber[5] first demonstrated the mechanism of TEI. Button[6] investigated the stability of the contact between two sliding half-planes using a perturbation method and showed that a small perturbation in the otherwise uniform contact pressure between two sliding half-planes can cause instability if the sliding speed exceeds a critical speed. Yi[7] implemented Burton's method numerically for the limiting case where the friction pads are non-conductors, in which case the perturbation is stationary with respect to the disc. Lee[8] solved the TEI problem by assuming that perturbations in the temperature and stress field increase exponentially with time. Recently, the finite element (FE) technique has been used to perform a transient analysis of thermoelastic contact problems with frictional heat generation. Zagrodzki[9] discretized both the thermoelastic contact problem and the transient heat conduction problem by using the two-dimensional axis-symmetric element, considering the migration of thermoelastic disturbance in the sliding direction. Choi[10] developed an FE model for an axis-symmetric coupled thermoelastic contact problem which simulated a disc brake and investigated the TEI phenomena of disc brakes during the drag braking process. Ahn[11] performed a transient FE simulation for the two-dimensional contact problem involving thermo-elastroplastic instability. These studies have limited application in the industry because the systems were assumed to represent a two-dimensional problem for just one-way coupling condition (mechanical to thermal analysis). On the other hand, Li[12] approximated the temperature and contact pressure distribution of a typical multidisc clutch system using the transient modal analysis method. Du[13] used the FE techniques to determine the critical speed by solving an eigen value problem based on Burton's perturbation method. This study shows weakness if the rotating speed of the disc

varies rapidly, in which case, convergence may not be reached.

In this study, a transient FE analysis method was used to analyze the fully coupled thermoelastic instability problem for a disc brake system. The three-dimensional mechanical and thermal models for the disc brake were generated separately, and solved iteratively using the staggered approach.[14] Brake dynamo tests are performed, and BTV and temperature variation of the disc are measured. Simulation and test results are compared, and the usefulness of the analysis method presented in this paper is discussed.

2. Theoretical Background

The equation of motion of a constrained dynamic system is introduced for the finite element approach;[15] more specific information can also be found in.[16,17] The general heat equation is briefly reviewed and the basic analysis strategy for the coupled thermo-mechanical system is described based on the staggered approach.

2.1 Dynamics of a constrained flexible multibody system

The constraints on the system are efficiently taken into account using the Augmented Lagrangian method. The augmented functional of Hamilton's principle is

$$\int_{t_1}^{t_2}\left[\delta(L-k\lambda^T\Phi-\frac{p}{2}\Phi^T\Phi)+\delta W\right]dt=0 \tag{1}$$

where k is s the scaling factor and p is the penalty coefficient. λ is the vector of Lagrange multipliers and Φ is the vector of constraints. L is the Lagrangian of the mechanism defined as $L=T-V$. T and V are the kinetic and potential energies of the system, respectively. W is the virtual work of external forces. The penalty coefficient p is generally chosen in terms of the characteristic stiffness of the system, and each constraint of the system can be affected to the penalty coefficient and scaling factor. At an equilibrium state, $k\lambda$ represents the reaction force of the constraints. The Augmented Lagrangian method tends to combine the advantage of the Lagrange Multiplier method and Penalty Function method. The term $k\lambda^T\Phi$ allows the constraints to be exactly imposed on the problem while p does not need to be infinite. At each iteration, $p\Phi^T\Phi$ reinforces the positive definiteness of the system matrix via the introduction of a moderate penalty coefficient p and scaling factor k. Using the virtual displacement principle, the motion equations are obtained as

$$\begin{cases}\dfrac{d}{dt}\left(\dfrac{\partial L}{\partial\dot{q}}\right)-\dfrac{\partial L}{\partial q}=Q-(k\lambda+p\Phi)\dfrac{\partial\Phi}{\partial q}\\ k\Phi(q,t)=0\end{cases} \tag{2}$$

where q is the vector of generalized coordinates. Eq. (2) can be written in the matrix form as

$$\begin{cases}M\ddot{q}+B^T(p\Phi+k\lambda)=g(q,\dot{q},t)\\ k\Phi(q,t)=0\end{cases} \tag{3}$$

where B is the gradient matrix of the constraints($B=\partial\Phi/\partial q$) and g is the vector of apparent force

$$g=Q-\frac{\partial L}{\partial q}-\frac{\partial}{\partial q}\left(\frac{\partial L}{\partial\dot{q}}\dot{q}\right) \tag{4}$$

The linearized form of the motion Eq. (2) can be described as

$$\begin{bmatrix}M & 0\\ 0 & 0\end{bmatrix}\begin{bmatrix}\Delta\ddot{q}\\ \Delta\ddot{\lambda}\end{bmatrix}+\begin{bmatrix}C_T & 0\\ 0 & 0\end{bmatrix}\begin{bmatrix}\Delta\dot{q}\\ \Delta\dot{\lambda}\end{bmatrix}+\begin{bmatrix}K_T & kB^T\\ kB & 0\end{bmatrix}\begin{bmatrix}\Delta q\\ \Delta\lambda\end{bmatrix}=\begin{bmatrix}r^*\\ -\Phi^*\end{bmatrix} \tag{5}$$

where r denotes the residual vector of equilibrium

$$r=g(q,\dot{q},t)-M\ddot{q}-B^T(p\Phi+k\lambda) \tag{6}$$

C_T is a tangent damping matrix obtained by differentiating the apparent force g with velocity vector $\dot{q}$

$$C_T=-\frac{\partial g}{\partial\dot{q}} \tag{7}$$

K_T is a tangent stiffness matrix resulting from the variation of the apparent force g, constraints Φ and mass matrix M with displacement vector q

$$K_T=-\frac{\partial g}{\partial q}+\frac{\partial(M\ddot{q})}{\partial q}+\frac{\partial(B^T(p\Phi+k\lambda))}{\partial q} \tag{8}$$

In this study, the differential-algebraic equations of motion of the system of Eq. (5) have been solved using the time integration scheme of Chung-Hulbert algorithm with the Newton-Raphson iteration.

2.2 Transient Computation of Heat transfer equation

The temperature within in an element is computed based on the nodal temperature vector

$$T(x,t)=\varphi(x)\cdot T(t) \tag{9}$$

where x is the nodal coordinate, $\varphi(x)$ is the interpolation function vector and $T(t)$ is the nodal temperature vector. The governing equation of the heat transfer problem is

$$C(T)\dot{T}+K(T)T=Q(T) \tag{10}$$

where $C(t)$ and $T(t)$ are the temperature-dependent heat capacity and thermal conductivity matrices, respectively, of the discretized system. T is the nodal temperature vector, $\dot{T}$ is the time derivative of the temperature vector, and $Q(t)$ is the heat flux vector. The solution vector T_γ of Eq. (10) at time γ, which is located at time intervals between the n and the $n+1$ step, can be expressed as

$$T_\gamma=(1-\gamma)T_n+\gamma T_{n+1} \tag{11}$$

The variation rate of the temperature can be written as

$$\dot{T}_\gamma=\frac{1}{\gamma\Delta t}(T_r-T_n) \tag{12}$$

Using Eq. (12), the equilibrium equations at time γ are

$$C(T_\gamma)\frac{T_\gamma-T_n}{\gamma\Delta t}+K(T_\gamma)T=Q(T_\gamma) \tag{13}$$

The solution T_γ is calculated iteratively as

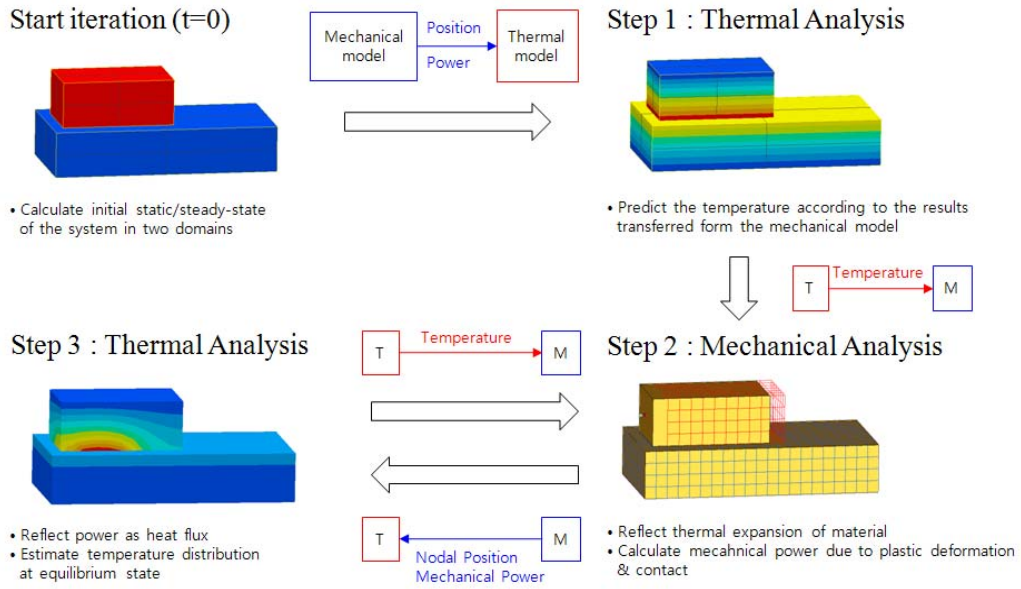

Fig. 1 Analysis strategy based on the staggered approach

$$T_{\gamma}^{i+1} = T_{\gamma}^{i} + \Delta T_{\gamma} \tag{14}$$

where the correction is calculated as

$$\Delta T_r = \frac{Q(T_r^i) - K(T_r^i)T_r - \dfrac{C(T_r^i)}{\gamma\Delta t}(T_r^i - T_n)}{K(T_r^i) + \dfrac{\partial K(T_r^i)}{\partial T}T_r + \dfrac{1}{\gamma\Delta t}\left(C(T_r^i) + \dfrac{\partial C(T_r^i)}{\partial T}T_r\right) - \dfrac{\partial Q(T_r^i)}{\partial T}} \tag{15}$$

Once the solution is known at time γ, one can obtain the solution at time n+1 as

$$T_{n+1} = T_n + \dot{T}_r \Delta t \tag{16}$$

In this paper, the Crank-Nicholson scheme is used to calculate the transient temperature of the system.

2.3 Heat generation due to frictional contact

In disc brakes, friction heat is generated between the disc and pads. Frictional heat generation per unit time at the node i is calculated as

$$q_{cf}{}^{i} = \eta\mu\sigma_c v \tag{17}$$

where η is the factor defining the percentage of mechanical power converted into heat, μ is the friction coefficient, σ_c is the contact pressure and v is the local velocity. The amount of heat going to the contractor and target bodies, $q_1{}^{i}$ and $q_2{}^{i}$, are determined with the parameter ω

$$q_1{}^{i} = \frac{\omega}{1+\omega} q_{cf}{}^{i}, \quad q_2{}^{i} = \frac{1}{1+\omega} q_{cf}{}^{i} \tag{18}$$

2.4 Analysis strategy based on the staggered approach

In the monolithic approach,[14] two different analysis domains such as the dynamic and thermal system are solved simultaneously and data is exchanged at the iteration level. Although the monolithic approach calculates the two fields in a unified domain and has the advantage of good convergence, it is expensive to compute. In the staggered approach, both domains are solved separately in succession always using the latest information provided from another part of the coupled system. This iteration is continued until convergence in the solution of the coupled equations is reached. The negative aspects of the staggered approach are that the convergence is not guaranteed and stability has to be determined. However, the staggered approach allows the use of the existing powerful software and it is relatively cheap to implement. The staggered approach is more suitable for solving large problems provided with contact conditions. This study analyzes the thermoelastic instability of disc brakes based on the staggered approach.

Fig. 1 shows the computational analysis strategy. The thermal model sends the nodal temperature distribution to the mechanical model, and the mechanical model transfers the nodal position and mechanical power to the thermal model. At time t = 0 s, the initial static state of the mechanical model and the initial steady-state of the thermal model are calculated. The initial position and power of the mechanical model are transferred to the thermal model. In step 1, the nodal temperature of the thermal model is updated considering the initial deformation and power of the mechanical model. In step 2, using the nodal temperature distribution, the amount of thermal expansion of the material is calculated. This expansion affects on the constraints including the contact condition. If the expansion of the material due to the temperature is too large, the Newton-Raphson iteration may fail to converge. The power due to plastic deformation and friction contact is computed in this step. In step 3, the power is changed to the heat flux and the heat flux is applied to the thermal model as a thermal load. In this step, the temperature distribution of the nodal point is estimated in equilibrium state. Steps 2 and 3 are repeated by the end of the simulation time. At every step, the time step is controlled automatically according to the residue of Eqs. (6) and (15) and if the residue does not converge in the allowed number of iterations, calculation stops.

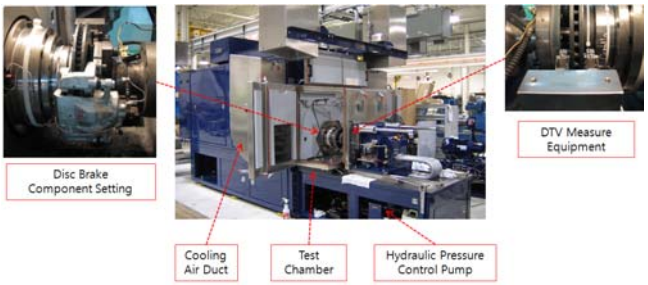

Fig. 2 Configuration of automotive inertia brake dynamometer model 300

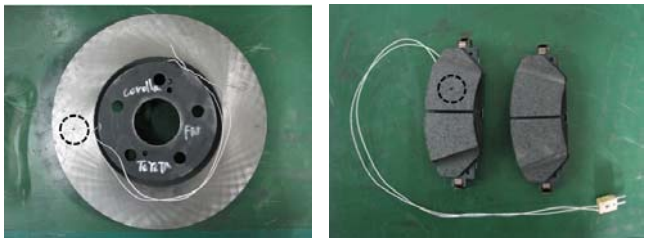

(a) Thermocouple in disc (b) Thermocouple in pads

Fig. 3 Thermocouples in disc and pads

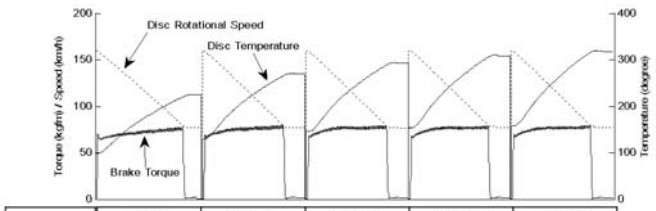

Result	1st braking			2nd braking			3rd braking			4th braking			5th braking		
	Max	Min	Diff	Max	Min	Diff	Max	Min	Diff	Max	Min	Diff	Max	Min	Diff
Temperature (℃)	225	99	126	271	131	140	294	146	148	311	154	157	321	158	163
Torque (Nm)	764.4	652.7	111.7	784.0	667.4	116.6	776.2	670.3	105.8	773.2	671.3	101.9	778.1	673.3	104.9

Fig. 4 Test results of 'Fade braking' mode

Table 1 Vehicle and brake information

	Category	Value
Vehicle information	Vehicle weight	14.05 kN
	Front axle weight	9.0 kN
	C.G height	549 mm
	Wheel base length	2650 mm
	Slip ratio	0.95
Brake information	Dynamic radius of tire	305 mm
	Diameter of wheel cylinder	57 mm
	No. of wheel cylinder	1 EA
	Brake effective radius	113 mm
	Brake effective factor	0.76
	Valve cut-in	294 N/cm^2

3. Brake Dynamo Test

3.1 Description of test environment

Brake dynamo test was done using LINK model 300. LINK model 300 can produce the maximum torque of 185 kW, and control the rotational speed of the disc up to 2000 rpm. Fig. 2 shows the dynamo test configuration. The disc brake component is equipped in the test chamber and connected with the driving motor. The air outside the building is pumped into the test chamber through the cooling air duct, and temperature and wind velocity in the chamber are controlled by adjusting the air flow. The hydraulic pressure control pump is used to control the pressure applied to the pad.

Fig. 3(a) and (b) show how thermocouples are inserted in disc and pads. Thermocouple is used to measure dynamic temperature variation of disc and pads. In Fig. 3(a), a thermocouple is inserted at the hole of the disc to a depth of 1 mm, and the hole is located at the center line of contact surface of the disc and pads. In Fig. 3(b), a thermocouple is inserted into the pad to a depth of 2 mm.

3.2 High speed judder test

Brake dynamo test was carried out according to the high speed judder test mode using the vehicle and brake information as shown in Table 1. The high speed judder test mode is widely applied for estimating the hot judder performance of a disc brake system. The high speed judder test is carried out as following procedure.

1) Initial measurement: The initial disc run-out, DTV and pad thickness are measured.
2) Pre-Burnish: The contact surfaces of disc and pad become to coincide, and then the '1st Judder' test is carried out.
3) 1st Judder test: Test results represent the initial judder performance of the disc.
4) 2nd Judder: there are two types of test modes- 'General braking' and 'Fade braking'. The 'Fade braking' test results are the most important, because hot spots occur on the disc surface most definitely during the 'Fade braking' mode. In the 'Fade braking' mode, the disc rotates with an initial rotational speed of 160 km/h, and then decrease to 80 km/h at a constant deceleration of 0.4g. This braking process is repeated five times at intervals of 90 seconds. In order to maintain the constant deceleration, the hydraulic pressure control pump controls the pad pressure.
5) Final measurement: The final disc run-out, DTV and pad thickness are measured.

Fig. 4 shows the test results of the 'Fade braking' mode. The disc rotational speed, disc temperature and brake torque were measured and are represented in Fig. 4. The disc temperature rises gradually according to time, and after the fifth braking, the disc temperature reaches its maximum temperature of 321℃. The BTV keeps a constant level of 101.9 ~ 116.6 Nm.

4. Hot Judder Simulation

The commercial finite element analysis code, SAMCEF, was used to perform the hot judder analysis of the disc brake system. A non-linear structural-dynamic model was created using SAMCEF/Mechano, and an unsteady state heat transfer model was created using SAMCEF/Thermal. The analysis results of the two models were exchanged using SAMCEF/Supervisor which is an intermediate processor based on 'Staggered approach'.

The hot judder simulation was performed in the fifth braking of the 'Fade braking' mode. 'Fade braking' includes five braking and

four intervals, and takes about 400 seconds. Thus, it took a long time to simulate the model for the entire time. Therefore, in this study, the fifth braking of the 'Fade braking' mode was selected since the hot spots appeared the most clearly at this braking. The simulation was performed by applying the initial data of the test results of the fifth braking to the model as initial conditions.

4.1 Description of test environment

Fig. 5 shows the finite element model of the disc brake system. The disc and pads are constructed using the 8-node hexahedron element. The disc consists of 24,048 nodes and 15,696 elements, and the pad consists of 2,250 nodes and 1,599 elements. The piston which applies the pressure to the pad is created using the 6-node pentahedron and 8-node hexahedron elements. The material properties of each model are shown in Table 2. In Table 2, the thermal expansion coefficient determines the amount of thermal expansion of the material, and makes the contact force between the disc and pads varied very sensitively. When a high thermal expansion coefficient is used, the contact force becomes very large and the equations of motion of a mechanical system may not converge. Thus, in this study, material properties of the disc and pads were obtained from the dynamic material tests.

4.2 Boundary conditions

Fig. 5 also shows the boundary conditions. In 'Fade braking', the vehicle speed varies from 160 km/h to 80 km/h with a constant deceleration of 0.4 g. The dynamic radius of a tire of 305 mm, slip ratio of 0.95, gravitational acceleration of 9.8 m/s^2 were used as vehicle data, to calculate the rotational speed of the disc as follows,

$$\mathrm{Rot}_{\mathrm{Initial}} = \left(160\times\frac{1000}{3600}\right)\Big/\left(2\times\pi\times\frac{305}{1000}\right)\times 60\times 0.95 = 1322(\mathrm{rpm})$$

$$\mathrm{Rot}_{\mathrm{Final}} = \left(80\times\frac{1000}{3600}\right)\Big/\left(2\times\pi\times\frac{305}{1000}\right)\times 60\times 0.95 = 661(\mathrm{rpm}) \quad (19)$$

$$\mathrm{T}_{\mathrm{Braking}} = \left[\left(160\times\frac{1000}{3600}\right)-\left(80\times\frac{1000}{3600}\right)\right]/9.8 = 5.67(\mathrm{s})$$

where $\mathrm{Rot}_{\mathrm{Initial}}$ and $\mathrm{Rot}_{\mathrm{Final}}$ are the initial and final rotational speed of the disc, and $\mathrm{T}_{\mathrm{Braking}}$ is the braking time. If the initial rotation speed of 1322 rpm is applied to the mechanical model as an initial condition, lots of calculation would be necessary to stabilize the model and convergence would not be guaranteed. Thus, the rotational speed of the disc increases from 0 rpm at t = 0 s to 1322 rpm at t = 0.1 s, and the speed is maintained for 0.1 second. The pad pressure is activated at t = 0.1 s, and the pad contacts the disc between t = 0.1 s and t = 0.2 s when the disc rotates at the constant speed of 1322 rpm. By making the pad contact the disc when the disc is at dynamic equilibrium, the solution of the dynamic equations of motion of the constrained multibody system presented in Part.1 can be obtained with small number of the Newton-Raphson iteration. The disc decelerates from 1322 rpm at t = 0.2 s to 661 rpm at t = 5.87 s at a constant deceleration of 0.4 g. The piston is fixed to the pad, and pressure of 30 bar is applied to the piston. The friction coefficient (μ) of 0.4 was set as the contact condition between the disc and pad. The average friction coefficient

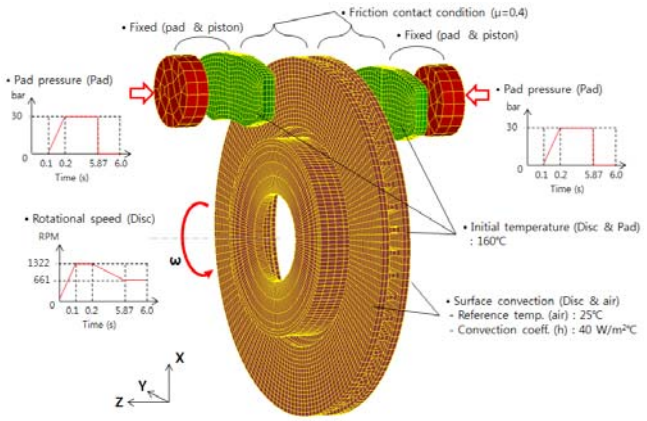

Fig. 5 Finite element model of the disc brake system for hot judder analysis

Table 2 Material properties of each component

Properties	Disc	Pad	Piston
Elastic modulus (GPa)	135	30	70
Poisson's ratio	0.29	0.3	0.33
Mass density (kg/m^3)	7,200	2,150	2,710
Thermal expansion coefficient (10^{-5}/℃)	1.05	0.76	2.3
Thermal conductivity (W/m℃)	53	1.5	177
Mass Capacity (J/kg℃)	642	465	875

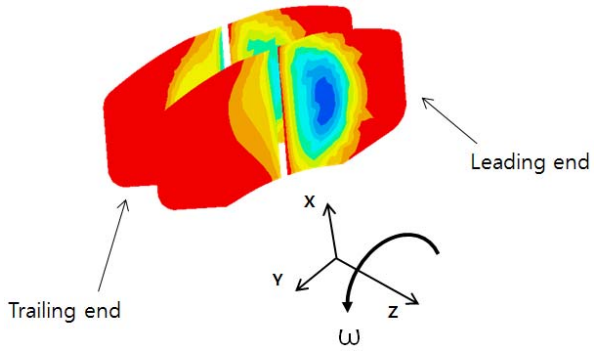

Fig. 6 Contact pressure distribution between the disc and pads

of 0.4 was obtained from the dynamo test results. The initial temperature of the disc and pad were 160 ℃, which is the first value of temperature from the result of the fifth braking test. The reference temperature of the air was 25 ℃ and the convection coefficient (h) was 40 W/m^2℃. The radiation between the disc and air was ignored.

4.3 Simulation result

If there is one piston in a caliper and the center axis of the piston is coincident with the center of mass of the pad, the pad pressure would be non-uniformly distributed.[18] Fig. 6 shows the contact pressure distribution between the disc and both pads. The contact pressure varies according to the rotational direction of the disc. The pressure of the region where the disc starts to contact the pad (leading end) is higher than that of the region where the disc ends contact with the pad (trailing end).

Fig. 7 shows the temperature distribution of the disc surface according to time. At each time step, following results are obtained.

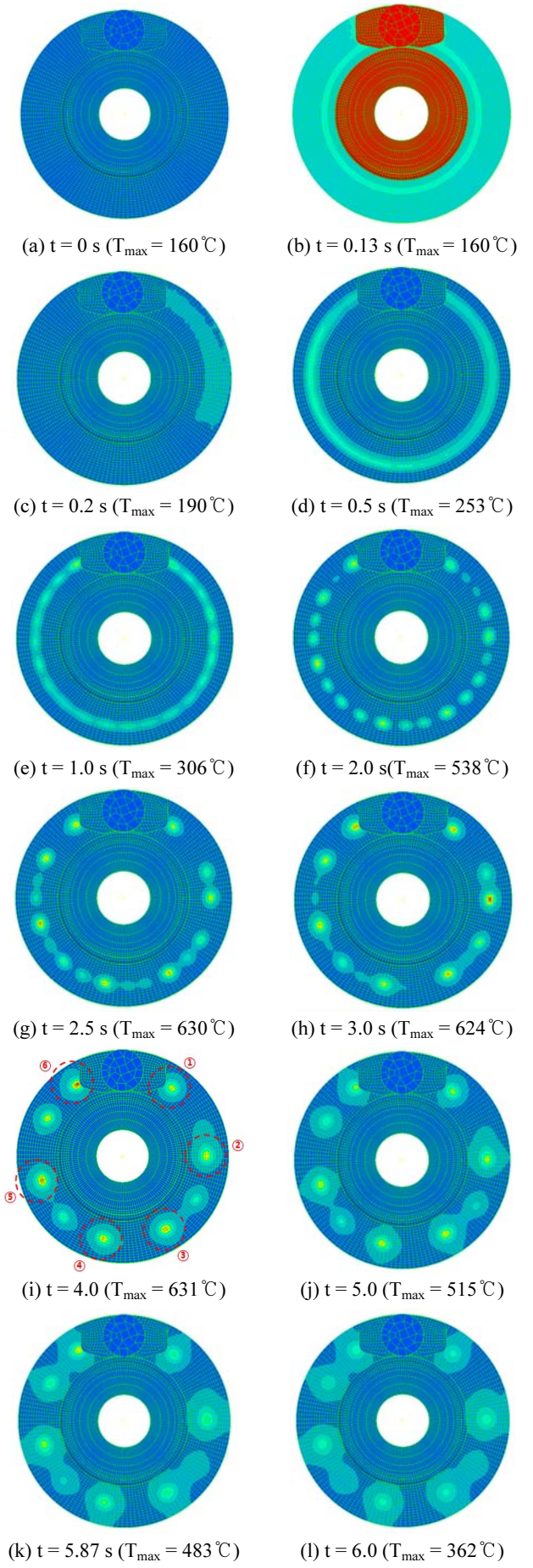

Fig. 7 Temperature distribution of the disc surface according to time

1) t = 0 s: The initial temperature of the disc is 160 ℃.
2) t = 0.13 s: Only convection heat transfer between the disc surface and air affects on the system. Contact between the disc and pad occurs after 0.13 s.
3) t = 0.2 s: Heat is generated by the friction contact between the disc and pad.
4) t = 0.5 s: Heat is generated along the center line of the contact surface. The maximum temperature of the band is 253℃.
5) t = 1.0 s: Regions of heat concentration are being created. Thermoelastic instability (TEI) is the main cause of this heat concentration.
6) t = 2.0 s ~ 3.0 s: Heat concentration is accelerated and these regions appear clearly.
7) t = 3.0 s ~ 4.0 s: Heat concentration develops to the hot spot. Six hot spots are generated and the maximum temperature of the center of the spots is 635℃.
8) t = 5.0 s: The temperature gradient around the hot spots becomes gentle. That is, the difference of temperatures between the center nodes of the hot spots and around the nodes decreases, because the rotating speed of the disc decreases. The maximum temperature of the hot spots is 585 ℃.
9) t = 5.87 s: Braking stops. Deceleration of the disc ends and there is no contact between the disc and pads. After this moment, the temperature of the disc decreases rapidly due to the convection between the disc surface and air.
10) t = 6.0 s: The maximum temperature of the disc reduces to 362 ℃. The temperature gradient at the hot spot becomes obscure.

5. Result comparison between simulation and dynamo test

To compare the simulation results to the dynamo test data, the disc temperature, BTV and DTV were obtained. The disc temperature was measured at the center node of the contact surface between the disc and pads. BTV was replaced by the reaction moment of the hinge joint applied at the rotation axis of the disc. The distance between two nodes, one at inboard and the other at outboard of the disc, is used as DTV. The two nodes are 10 mm far from the outer circle of the disc.

Fig. 8 shows the change of the disc temperature according to time. In Fig. 8, the solid line represents the simulation and the dashed line represents the dynamo test data. The disc temperature, whose initial value is 160 ℃, increases linearly, and reaches 320 ℃ at the end of braking. The maximum temperatures of the disc are 321 ℃ and 335.6 ℃ at the dynamo test and simulation, respectively. The error of the temperatures is only 1.4 %, and thus it is concluded that the simulation result is very reliable.

Fig. 9 shows the BTV results of the simulation and dynamo test. In Fig. 9, the solid line represents the simulation result and the dashed line represents the dynamo test data. In order to verify how

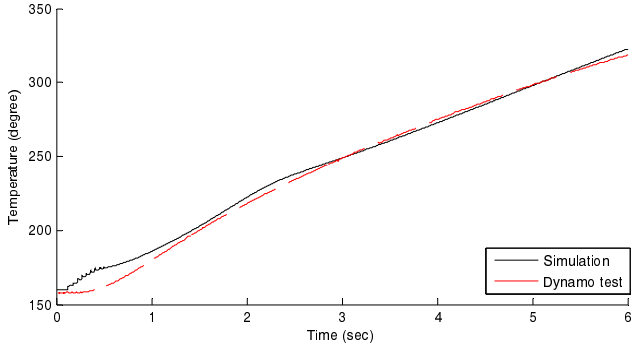

Fig. 8 Disc temperature variation according to time

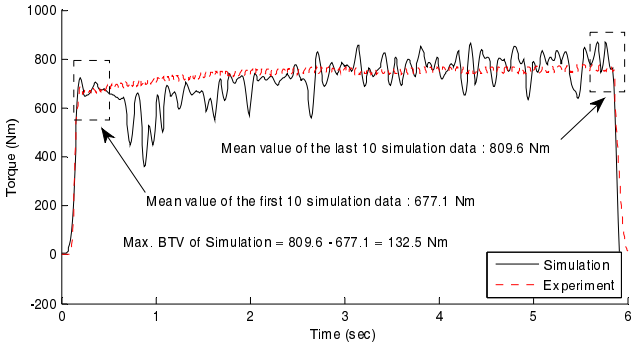

Fig. 9 Brake torque variation (BTV) according to time

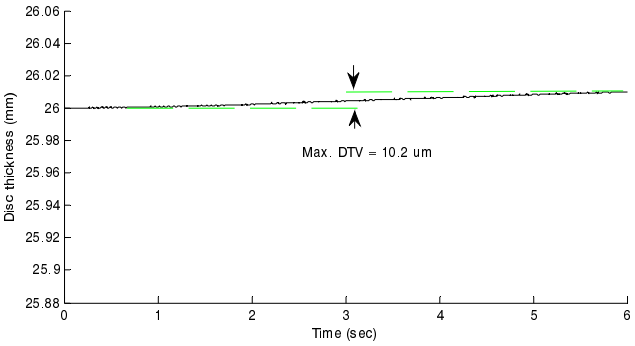

Fig. 10 Disc thickness variation (DTV) according to time

well the simulation results match with the test data, the Pearson correlation coefficient[19] and root mean square (RMS) values of data, which was obtained during braking as shown in Fig. 9, were calculated. The Pearson correlation coefficient was 0.741, and thus one can say that two data have a positive and strong linear relationship. The RMS values of the simulation and dynamo test were 722.5 Nm and 742.0 Nm, and the error was 2.6 %. Therefore, the BTV result of the simulation model followed the test data successfully. The maximum BTV of the dynamo test was 104.9 Nm. The maximum BTV of the simulation results, which was determined by the difference of the mean values of the first and last 10 simulation data as shown in Fig. 9, was 132.5 kgf, and this is very close to the test data.

Fig. 10 shows the DTV results of the simulation. The disc thickness, whose initial value was 26 mm, changed according to time, and the maximum DTV was 10.2 μm. The dynamic DTV of the dynamo test could not be measured since the sampling rate of the gap sensor was lower than the rotational speed of the disc. DTV of 10.2 μm was also very close to the actual value measure from the normal ventilated disc brakes.[20]

6. Conclusion

In this study, hot judder of a ventilated disc brake system was simulated. Based on the analysis technique presented in part.1 of this paper, the mechanical and thermal models of an actual brake system were created, and simulated using the analysis module of SAMCEF. During simulation, six hot spots were generated on the surface of the disc. These hot spots are very important contribution of this paper since no previous studies could produce hot spots. Brake dynamo test was done according to the high speed judder test mode, and simulation and test results such as the variation of the disc temperature and brake torque were compared with the test data. The disc temperature shows only 1.4 % difference between the simulation and test, and BTV of the simulation model agreed well with the actual BTV with an error of 0.17 %. DTV obtained from simulation was 10.2 μm, and this value is very close to the actual value of the normal disc brake system. Therefore, the simulation technique and hot judder analysis model presented in this paper were verified. For the future work, an optimization of the shape of the ventilated disc will be performed by using the response surface methodology,[21] and the results will be verified.

REFERENCES

1. Lee, K. J. and Barber, J. R., "An Experimental Investigation of Frictionally-Excited Thermoelastic Instability in Automotive Disk Brakes Under a Drag Brake Application," Journal of Tribology, Vol. 116, No. 3, pp. 409-414, 1994.
2. Altuzarra, O., Amezua, E., Aviles, R. and Hernandez, A., "Judder Vibration in Disc Brakes Excited by Thermoelastic Instability," Engineering Computations, Vol. 19, No. 4, pp. 411-430, 2002.
3. Jang, Y. H. and Ahn, S. H., "Frictionally-excited Thermoelastic Instability in Functionally Graded Material," Wear, Vol. 262, No. 9-10, pp. 1102-1112, 2007.
4. Yi, B. Y., Barber, J. R. and Zagrodzki, P., "Eigenvalue Solution of Thermoelastic Instability Problems using Fourier Reduction," Proc. of the Royal Society of London A, Vol. 456, pp. 2799-2821, 2000.
5. Barber, J. R., "Thermoelastic Instabilities in the Sliding of Conforming Solids," Proc. of the Royal Society of London A, Vol. 312, pp. 381-394, 1969.
6. Burton, R. A., Nerlikar, V. and Kilaparti, S. R., "Thermoelastic Instability in a Seal-like Configuration," Wear, Vol. 24, No. 2, pp. 177-188, 1973.
7. Yi, Y. B., Du, S., Barber, J. R. and Fash, J. W., "Effect of Geometry on Thermoelastic instability in Disk Brakes and

Clutches," Journal of Tribology, Vol. 121, No. 4, pp. 661-666, 1999.

8. Lee, K. J. and Barber, J. R., "Frictionally Excited Thermoelastic Instability in Automotive Disk Brakes," Journal of Tribology, Vol. 115, No. 4, pp. 607-614, 1993.
9. Zagrodzki, P., Lam, K. B., Bahkali, E. A. and Barber, J. R., "Nonlinear Transient Behavior of a Sliding System With Frictionally Excited Thermoelastic Instability," Journal of Tribology, Vol. 123, No. 4, pp. 699-708, 2001.
10. Choi, J. H. and Lee, I., "Transient Thermoelastic Analysis of Disk Brakes in Frictional Contact," Journal of Thermal Stresses, Vol. 26, No. 3, pp. 223-244, 2003.
11. Ahn, S. H. and Jang, Y. H., "Frictionally Excited Thermo-elastoplastic Instability," Tribology International, Vol. 43, No. 4, pp. 779-784, 2010.
12. Li, J. and Barber, J. R., "Solution of Transient Thermoelastic Contact Problems by the Fast Speed Expansion Method," Wear, Vol. 265, No. 3-4, pp. 402-410, 2008.
13. Du, S. and Fash, J. W., "Finite Element Analysis of Frictionally-excited Thermoelastic Instability in 3D Annular Disk," International Journal of Vehicle Design, Vol. 23, No. 3-4, pp. 203-217, 2000.
14. Yoon, G. H. and Sigmund, O., "A Monolithic Approach for Topology Optimization of Electrostatically Actuated Devices," Computer Methods in Applied Mechanics and Engineering, Vol. 197, No. 45-48, pp. 4062-4075, 2008.
15. Cardona, A., "An Integrated Approach to Mechanism Analysis," Ph.D. Thesis, Aerospace & Mechanical Engineering, University of Liege, Belgium, 1989.
16. Geradin, M. and Cardona, A., "Flexible Multibody Dynamics," John Willey & Sons, pp. 10-137, 2000.
17. Doan, D. B., "Modeling and Analysis of Landing Gears," Ph.D. Thesis, Aerospace & Mechanical Engineering, University of Liege, Belgium, 2004.
18. Limpert, R., "Brake Design and Safety, 2nd edition," Society of Automotive Engineers, Inc., pp. 54-57, 1999.
19. Ahlgren, P., Jarneving, B. and Rousseau, R., "Requirements for A socitation Similarity Measure, with Special Reference to Pearson's Correlation Coefficient," J. Amer. Soci. Info. Sci. Tech., Vol. 54, No. 6, pp. 550-560, 2003.
20. Kao, T. K., Richmond, J. W. and Douarre, A., "Brake Disc Hot Spotting and Thermal Judder: an Experimental and Finite Element Study," International Journal of Vehicle Design, Vol. 23, No. 3-4, pp. 276-296, 2000.
21. Jung, S. P., Park, T. W., Yoon, J. W., Jun, K. J. and Chung, W. S., "Design Optimization of Spring of a Locking Nut using Design of Experiments," Int. J. Precis. Eng. Manuf., Vol. 10, No. 4, pp. 77-83, 2009.